JOURNAL OF AIRCRAFT
Vol. 39, No. 2, March–April 2002

Computational Fluid Dynamics Evaluation of National Aerospace Laboratory Experimental Supersonic Airplane in Ascent

Takeshi Fujita,* Yasushi Ito,* and Kazuhiro Nakahashi†
Tohoku University, Sendai 980-8579, Japan
and
Toshiyuki Iwamiya‡
National Aerospace Laboratory, Mitaka 181-0015, Japan

Aerodynamic coefficients of the National Aerospace Laboratory experimental airplane piggybacked on a solid rocket booster in ascent are numerically evaluated by solving the Euler equations on unstructured tetrahedral grids. For accurate representation of the configuration, a computational method has been developed. The method effectively links a computer-aided-design-based modeling to the efficient surface meshing. It also enables quick addition/removal of the small components attached on the original model to investigate their aerodynamic effects. The computed lift coefficients show good agreement with wind-tunnel data in all regions of flight speed from transonic to supersonic flow. It is made clear that a small component affects physical phenomena the flowfield, and as a consequence, the total aerodynamic performance of the airplane is largely changed. It is concluded that the detailed representation of the original geometry is very important for accurate evaluation of the transonic lift coefficients.

Introduction

THE National Aerospace Laboratory (NAL) has established a research program for scaled experimental supersonic airplanes.[1] The first model of the experimental airplanes is unpowered and will be launched by a solid rocket booster in 2002. The airplane will be released from the rocket booster at altitude of 15,000 m and a Mach number of 2.5, and then the airplane will be gliding for flight tests. The aerodynamic configuration with no propulsion system was designed in a two-stage process. First, a baseline configuration was designed using a conventional linearized theory. Then, computational fluid dynamics (CFD) and a supersonic inverse method[2] were used to refine the wing geometry and to achieve a higher lift-to-drag ratio at a design point of a freestream Mach number M_∞ of 2.0 and lift coefficient C_L of 0.1. To reduce drag, the experimental airplane was designed to realize the natural laminar flow on the upper surface of the wing.[3]

For the success of this flight experiment, it is important to predict aerodynamic interference between the airplane and the rocket during the separation process, as well as aerodynamic performances from transonic to supersonic regimes. This paper reports the detailed numerical analysis and compares the results with wind-tunnel experimental data. The aerodynamic performance had been investigated in the wind tunnel at the NAL.

In the present paper, tetrahedral unstructured grid is used to discretize the flowfield. A seamless procedure to transfer geometrical data from the modeling by a computer-aided-design (CAD) system to the surface/volume grid generation has been developed to reconstruct accurately the complex configuration in the computational space. The present paper discusses the procedure to utilize a CAD system to model and to modify a geometry as the preprocessing of the grid generation and flow computations. The method is demonstrated for the numerical evaluation of the aerodynamic coefficients of the NAL experimental airplane piggybacked on the rocket booster. The procedure is also useful to investigate the sensitivity of aerodynamic coefficients to the presence of small components in the detailed configuration, such as pitot tube, etc.

CAD Modeling

Semispan configurations of an experimental supersonic airplane and a rocket booster are shown in Fig. 1. The fuselage length of the airplane is 11.5 m, and the span is 4.718 m. The models were defined at the NAL using CATIA, which is a commercial CAD system. The CAD models include detailed parts, such as a pitot tube on the airplane and pipe covers and connecting parts on the rocket booster, as shown in Fig. 1. To compute flows around such a complex configuration, a seamless procedure from the CAD output to the surface meshing is required for the precise surface reconstruction of the original CAD-defined model in the computational space. Here CATIA is used to build the models and to modify them to adjust them to the CFD grid. The CAD is also used to remove small parts on the rocket booster to investigate their effects on aerodynamic coefficients.

The experimental airplane and the rocket booster were defined independently by CAD. Then, they were connected, as shown in Fig. 1. To use this CAD model for unstructured grid generation, the model must be defined by a watertight surface that has no gap and no overlapping between components. In the present model, the following four regions of the configuration were modified on CATIA: 1) static pressure holes in the pitot tube ahead of the airplane, 2) small gaps at the connecting components between the airplane and the rocket booster, 3) finite thickness at trailing edges of wings, and 4) patched surface (called FACE or SURFACE in CATIA).

The static pressure holes and the small gaps at the connecting parts are so small that they do not affect the flowfield. However, these small holes and gaps sometimes cause difficulties in generating the grids and in the flow computations. Therefore, these holes and gaps were closed, as shown in Fig. 2.

The finite thickness of the trailing edge for the present model is 0.013% of the chord length at the wing root and 0.11% at the wing tip, as shown in Fig. 3. This very thin surface would create very high aspect ratio triangles or very small triangles in the surface grid

Received 27 July 2001; revision received 29 October 2001; accepted for publication 1 November 2001.

*Graduate Student, Department of Aeronautics and Space Engineering, Aoba-yama 01.
†Professor, Department of Aeronautics and Space Engineering, Aoba-yama 01. Associate Fellow AIAA.
‡Director, Computational Fluid Dynamics Technology Center, 6-13-1 Osawa. Member AIAA.

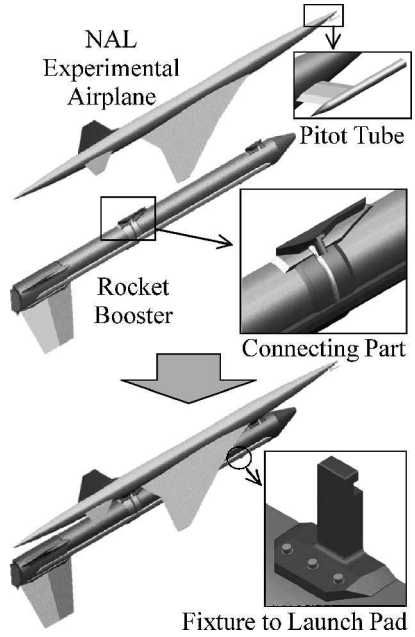

Fig. 1 Superposition of two CAD models.

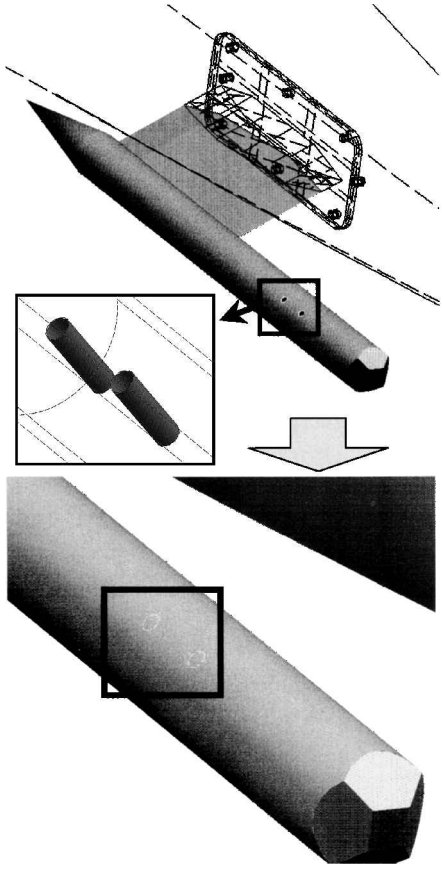

Fig. 2 Static pressure holes at pitot tube.

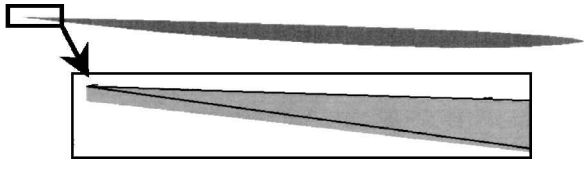

Fig. 3 Thickness at trailing edge.

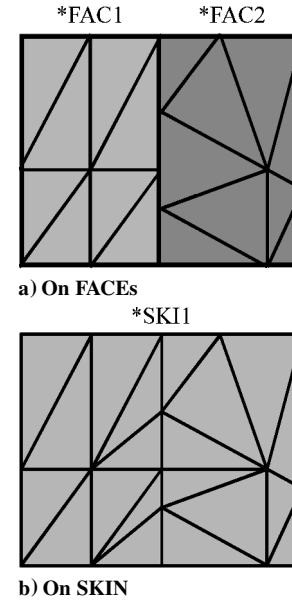

Fig. 4 STL facets on FACEs and a SKIN.

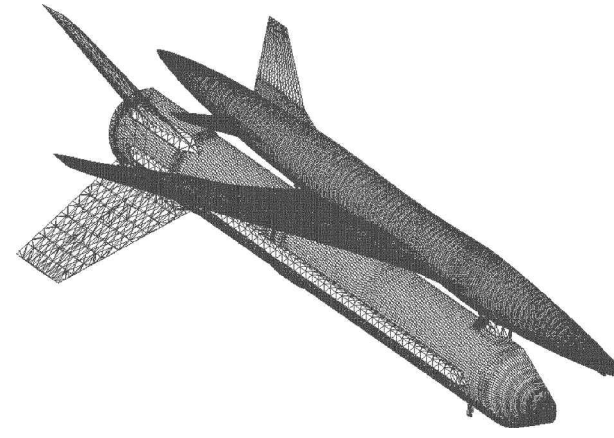

Fig. 5 STL data.

generation. To avoid this, the trailing edge of the wing is sharpened, as shown in Fig. 3.

Item 4 about the patched surface is the most important procedure when CATIA is used as the surface modeling for the surface grid generation. In the present method, the CAD data are transferred to the surface grid generator by the stereolithography (STL) output format, which is made from pure geometric information composed of triangular facets and their associated unit normal. The STL file is employed here as a background grid for the surface meshing. Therefore, this background grid defined by the STL file must cover the original surface without overlaps or gaps. Usually, a configuration is defined by sets of FACES and SURFACES in CATIA.[4] The CATIA has information about connection of each surface, but the information is lost at the boundary of each surface when the STL file is generated (Fig. 4a). To keep this information, SKIN or VOLUME should be created. SKIN is a general set of joined faces, and VOLUME is the part of a space bounded by a set of joined faces. The data SKIN does not have to be closed, but VOLUME must be closed. The data SKIN is used for a half-model. If the STL triangles are created on only one SKIN or VOLUME, a set of triangles is generated, as shown in Fig. 4b.

Surface/Volume Grid Generation

To generate a surface grid, the STL data generated by CAD is needed (Fig. 5). The STL data format is designed for rapid prototyping and represents a surface via a set of triangular facets.[5] These data contain only pure geometric information of the model so that it is easily manipulated.

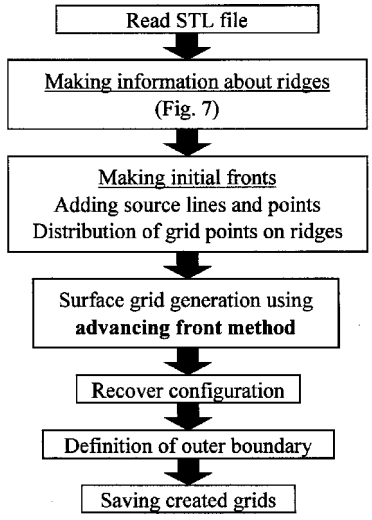

Fig. 6 Flowchart of surface grid generation.

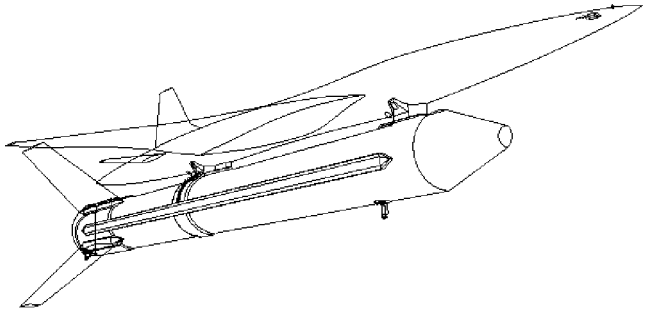

Fig. 7 Reconstruction of geometric features.

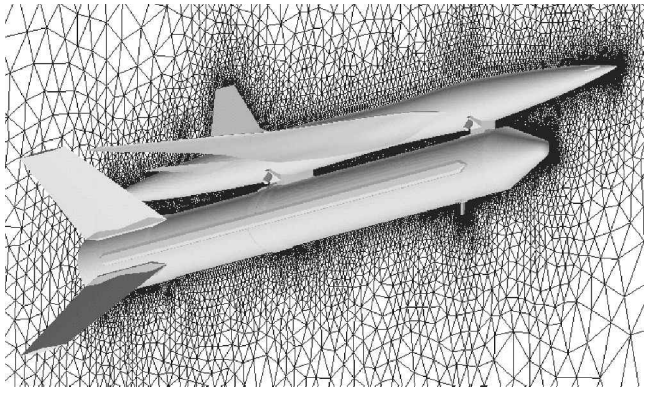

Fig. 8 Volume grid.

The Edge Editor, a surface meshing software developed at Tohoku University,[6] was used to generate the surface grid with STL data of the NAL experimental airplane. The flowchart of the surface grid-generation procedure is shown in Fig. 6. After the geometry data are read, preprocessing is performed before the surface meshing. This procedure constructs geometrical feature lines, as shown in Fig. 7, as well as a background grid for surface meshing. Then, using the feature lines as the initial fronts, the advancing front algorithm is applied to the background grid. The volume grid (Fig. 8) is finally generated by Delaunay tetrahedral meshing (see Ref. 7). For the present model, shown in Fig. 1, the surface grid has 117,561 nodes and 235,118 triangles. The volume grid contained 658,532 nodes and 3,570,327 tetrahedral elements.

Flow Solver

The Euler equations are solved by a solution algorithm based on the finite volume cell-vertex scheme for arbitrary shaped cells.[8] The control volume is no overlapping dual cells constructed around each node. To enhance the accuracy, a linear reconstruction of the primitive variables inside the control volume is applied with Venkatakrishnan's limiter.[9] The flux is computed using a Harten–Lax–van Leer–Einfeldt–Wada approximate Riemann solver (see Ref. 10). The computational efficiency is improved by the lower–upper symmetric Gauss–Seidel implicit method with a reordering algorithm (see Ref. 8) for unstructured grids. This implicit time integration method does not require extra storage, and its performance is similar to that of structured grid schemes.

Computational Results

A. Aerodynamic Coefficients of Full Configuration

The computed pressure distribution on the airplane with the rocket booster, as well as the pressure contours on the symmetry plane, is shown in Fig. 9. The freestream Mach number is 1.05, and the angle of attack is zero. The computed pressure distribution at Mach 2.0 is shown in Fig. 10. The pitot tube near the nose of the experimental airplane and the connecting parts between the airplane and the rocket booster are found to create shock waves. A relatively strong shock wave generated at the nose of the booster reflects on the lower surface of the airplane.

In Fig. 11, the computed C_L is compared with the result of wind-tunnel data, obtained at the NAL. To check grid dependency, the result obtained by a fine grid, which contains 1,016,074 nodes, is also shown. Two grids, one with 0.66×10^6 nodes and the other with 1.02×10^6 nodes, give similar results. Therefore, we conclude that the grid with 0.66×10^6 nodes is sufficient to predict accurately aerodynamics forces.

The lift coefficient has the peak value at the transonic regime. Then it gradually decreases as the freestream Mach number increases. Although the overall agreement is very good, there is about

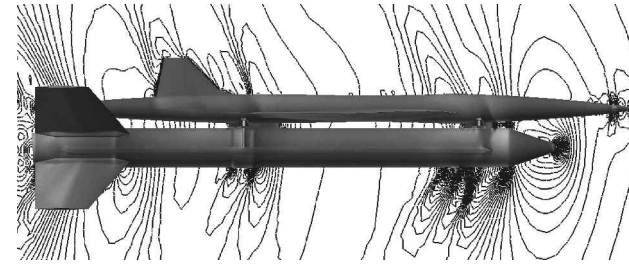

Fig. 9 Computed pressure contours at $M_\infty = 1.05$.

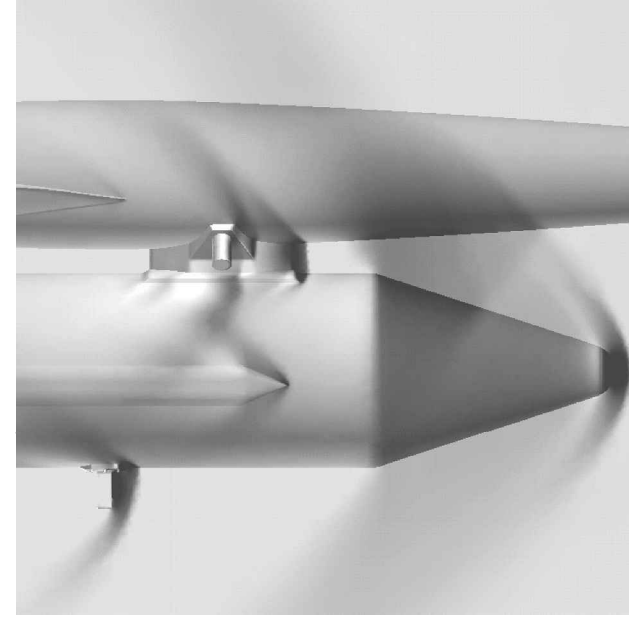

Fig. 10 Computed pressure distribution at $M_\infty = 2.0$.

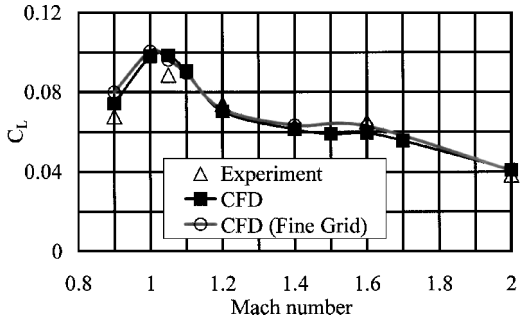

Fig. 11 Comparisons of lift coefficients.

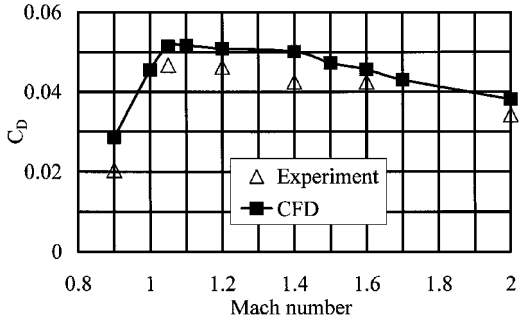

Fig. 12 Comparisons of drag coefficients.

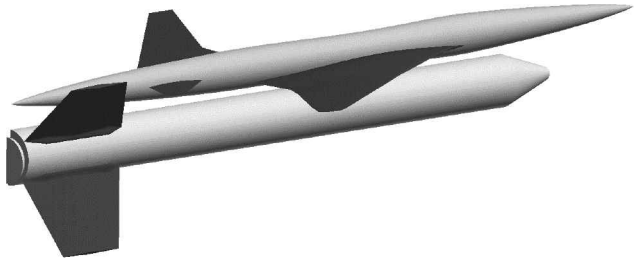

Fig. 13 Simplified configuration.

a 10% difference between the experimental data and the computed results at a freestream Mach number of 1.05. This discrepancy is mainly due to the inability of the Euler computation to simulate the shock–boundary-layer interactions whose effect becomes large at the transonic regime. In the supersonic regime, the differences between the experiment and the computation are less than 6%. The computed results show good agreements with wind-tunnel results even with the inviscid flow assumption.

The drag coefficient C_D is compared with the experiment in Fig. 12. To compare the experimental data with the present inviscid flow results, the experimental values in Fig. 12 were modified by subtracting the approximated frictional drag for a flat plate. The base pressure contribution was also removed in C_D computations.

B. Sensitivity of Aerodynamic Coefficients to Small Components

The model shown in Fig. 1 has several small components, such as pitot tube, connecting parts between rocket booster and airplane, fixtures to launch pad, and casing on the side of the booster. These small parts generate various shock waves, which interact each other between the airplane and the rocket booster, as shown in Fig. 10. Therefore, it is valuable to estimate aerodynamic effects of these small components beforehand in designing the entire piggybacked configuration. For this purpose, the present procedure of coupling the unstructured grid CFD with the CAD system provides a very useful engineering tool.

To investigate aerodynamic effect of these small components, a simplified configuration without any small components was prepared by CATIA (Fig. 13). The computed pressure contours of the simplified configuration, corresponding to Fig. 9 of the fully detailed configuration, are shown in Fig. 14. The freestream Mach number is 1.05, and the angle of attack is zero. When the computed pressure contours for the simplified configuration as shown in Fig. 14 is compared with those for the detailed configuration as shown in Fig. 9, the shock wave formation for each case is found to be quite different from each other.

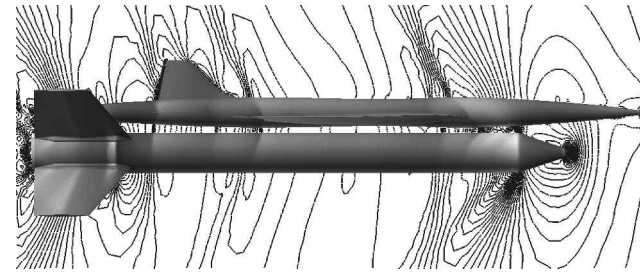

Fig. 14 Computed pressure contours of simplified configuration at $M_\infty = 1.05$ and $\alpha = 0$ deg.

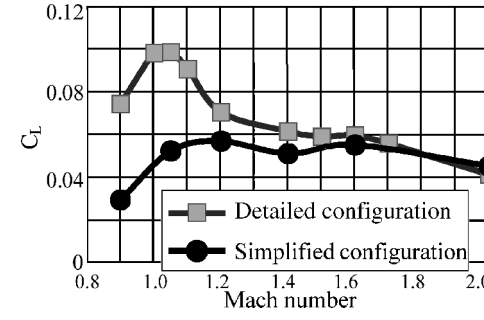

Fig. 15 Lift coefficients of precise model and simplified one.

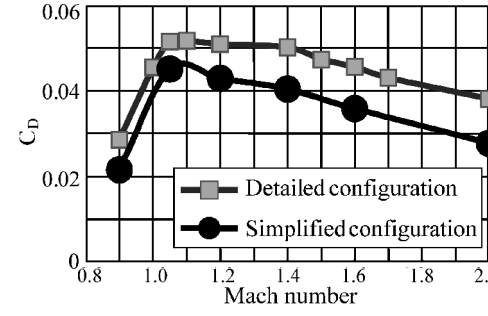

Fig. 16 Drag coefficients of precise model and simplified one.

The lift coefficient and the drag coefficient of the simplified configuration were also compared with the detailed one, as shown in Figs. 15 and 16. The difference of the lift coefficients between the two is about 50% in the transonic flow regime. Although the removed parts in the simplified configuration are very small compared with the fuselages and the wings, its effects on the lift coefficients are quite large.

The reason for the difference in lift coefficient is that a shock wave is generated due to the existences of the small components, and it significantly alters the pressure distribution on the lower surface of the main wing. Actually, Fig. 17 clearly shows a shock wave at the lower surface of the main wing of the detailed configuration.

Comparison of pressure distributions between the detailed and simplified configuration on the main wing at the spanwise sections α and β are shown in Fig. 18. Pressure distributions are substantially different due to the shock wave on the lower surface. Lift is produced by the subtraction between the pressure coefficient distribution on the lower surface and the one at the upper surface. The pressure increase after the shock wave on the lower surface leads to C_L increases. This causes a significant increase of C_L in Fig. 15 at the transonic regime.

C. Effects of Front and Rear Connecting Parts

To identify the component that causes the lift increase at the transonic regime, two configurations were modeled by CATIA: One is the simplified configuration with the front connecting part (Fig. 19a),

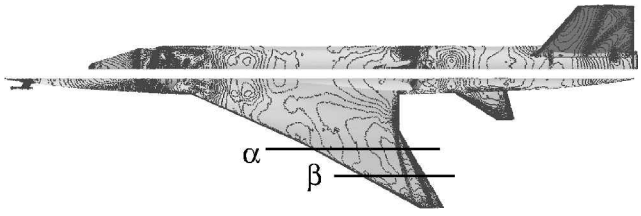

a) Detailed configuration

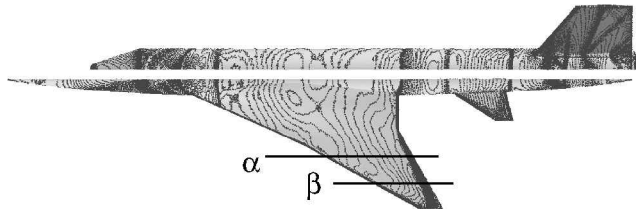

b) Simplified configuration

Fig. 17 Pressure contours on lower surface of airplane and upper surface of booster at $M_\infty = 1.05$.

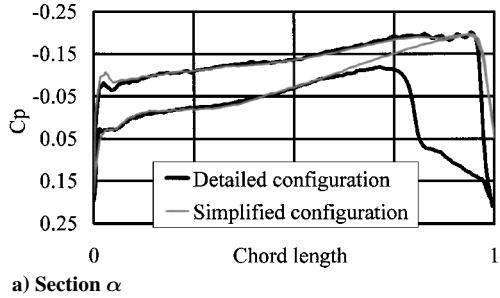

a) Section α

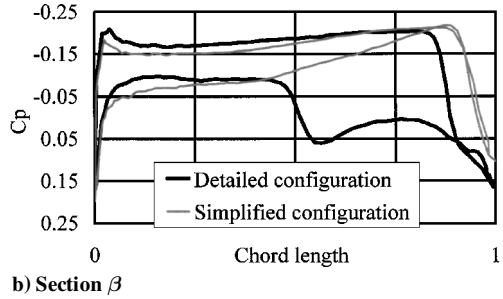

b) Section β

Fig. 18 C_P distributions on main wing at $M_\infty = 1.05$.

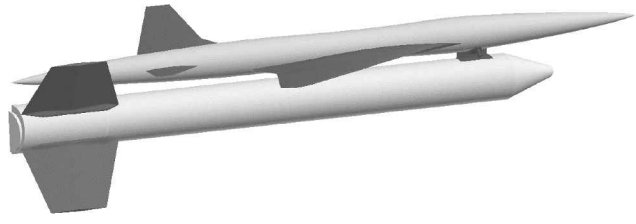

a) Simplified configuration with front connecting part

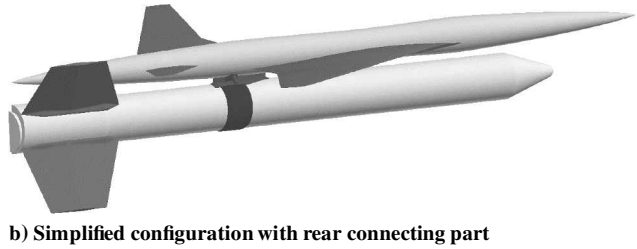

b) Simplified configuration with rear connecting part

Fig. 19 Two geometries with connecting parts.

and another is the simplified one with the rear connecting part (Fig. 19b). These modifications of the configuration are straightforward for the CATIA operator. Flows around each of the two configurations were computed using the unstructured grid CFD, and the lift coefficients are compared in Figs. 20 and 21. We also evaluated aerodynamic effects of the front and rear connecting parts.

As shown in Fig. 20, the lift coefficient of the configuration with the front connecting part is similar to the simplified one. The front connecting part does not affect the total lift coefficient very much. On

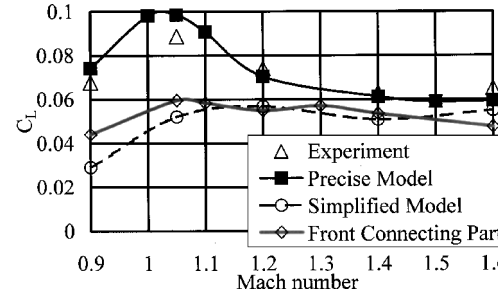

Fig. 20 Effect of front connecting part on C_L.

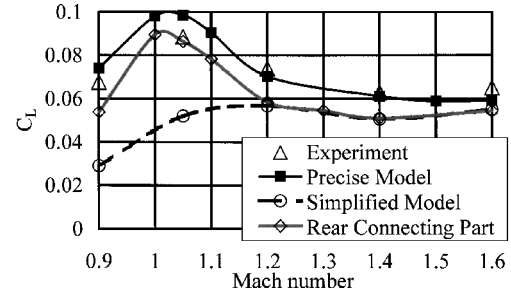

Fig. 21 Effect of rear connecting part on C_L.

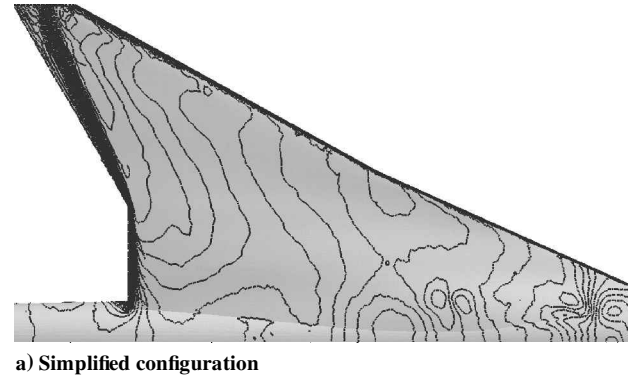

a) Simplified configuration

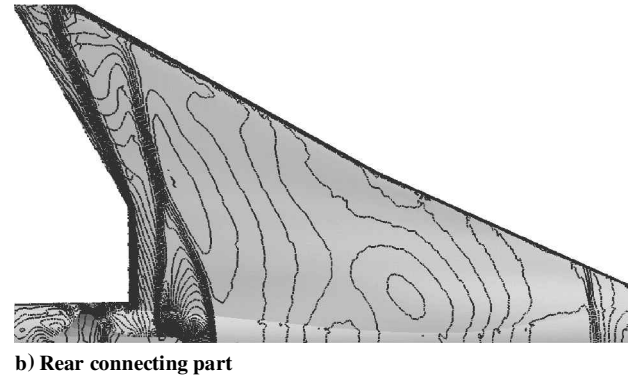

b) Rear connecting part

Fig. 22 Pressures contour on lower surface of main wing at $M_\infty = 1.05$.

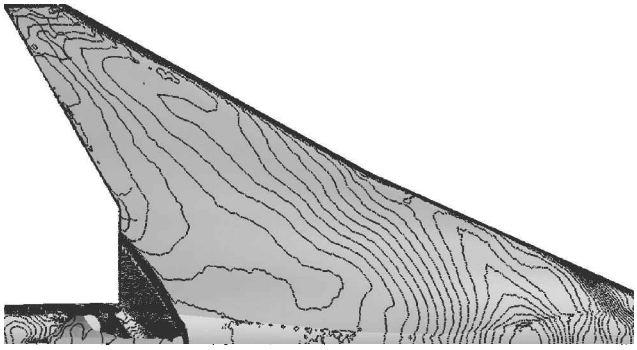

Fig. 23 Pressure contours on lower surface of main wing of the simplified configuration with the rear connecting part at $M_\infty = 1.4$.

the other hand, the rear connecting part significantly increases the lift in the transonic regime (Fig. 21). The lift increase at the transonic regime is mainly caused by the existence of the rear connecting part.

Figure 22 shows pressure contours on the lower surface of the main wing. Figure 22a shows the contours for the one about the simplified configuration without any small components at a freestream Mach number of 1.05. A shock wave can be observed only at the trailing edge of the wing. Figure 22b shows the contours for the configuration with the rear connecting part. A shock wave is generated upstream of the rear connecting part, and it reaches at the tip of the wing. At a freestream Mach number of 1.4, as shown in Fig. 23, although the shock wave is generated, it leans downstream. Therefore, its effect on the lift coefficient is small.

Conclusions

Aerodynamic coefficients of the NAL experimental airplane piggybacked on a solid rocket booster in ascent have been numerically evaluated by solving the Euler equations and have been compared with wind-tunnel data. The detailed configuration was defined by CATIA, and the surface grids were generated directly from the CATIA-defined surfaces using the STL output. The computed results show good agreement with wind-tunnel results in terms of lift and drag coefficients from the transonic to supersonic flow regimes.

A combination of the CAD-based modeling and the efficient surface meshing allows us to add/remove small attachments easily in the detailed configuration for computations. Then, we can investigate each attachment aerodynamic effects using trial-and-error computation, in a short period. In a trial-and-error process, the simplified configuration, where small attachments were removed, was also calculated. The two computed results, one with a small attachment and the other without one, show significant changes in the transonic lift coefficients. The small connecting part attached on the rocket booster generates shock waves on the lower surface of the airplane wing, resulting in drastic changes in pressure distributions on the wing. Thus, we conclude that to perform reliable and accurate simulation precise geometrical representation of an aircraft is important. For the precise representation, the proposed method is a most useful strategy for the preprocess of grid generation.

References

[1]Iwamiya, T., "NAL SST Project and Aerodynamic Design of Experimental Aircraft," *Proceedings of the 4th ECCOMAS Computational Fluid Dynamics Conference*, Wiley, Chichester, England, U.K., 1998, pp. 580–585.

[2]Matsushima, K., Iwamiya, T., and Ishikawa, H., "Supersonic Inverse Design of Wings for the Full Configuration of Japanese SST," *Proceedings of the 22nd International Congress of Aeronautical Sciences*, ICAS 2000-2.1.3, Aug.–Sept. 2000, pp. 1–8.

[3]Shimbo, Y., Yoshida, K., Iwamiya, T., Takaki, R., and Matsushima, K., "Aerodynamic Design of the Scaled Supersonic Experimental Airplane," *Proceedings of the 1st International CFD Workshop for Super-Sonic Transport Design*, Tokyo, Japan, 1998, pp. 62–67.

[4]"Motif CATIA Solutions, User's Guide UNIX Workstation," Dassault Systems, 1995.

[5]"Stereolithography Interface Specification," 3D Systems, Inc., CA, 1989.

[6]Ito, Y., and Nakahashi, K., "Direct Surface Triangulation Using Stereolithography (STL) Data," AIAA Paper 2000-0924, Jan. 2000.

[7]Sharov, D., and Nakahashi, K., "A Boundary Recovery Algorithm for Delaunay Tetrahedral Meshing," *Proceedings of the 5th International Conference on Numerical Grid Generation in Computational Field Simulation*, International Society of Grid Generation, MS, April, 1996, pp. 229–238.

[8]Sharov, D., and Nakahashi, K., "Reordering of Hybrid Unstructured Grids for Lower–Upper Symmetric Gauss-Seidel Computations," *AIAA Journal*, Vol. 36, No. 3, 1998, pp. 484–486.

[9]Venkatakrishnan, V., "On the Accuracy of Limiters and Convergence to Steady-State Solutions," AIAA Paper 93-0880, Jan. 1993.

[10]Obayashi, S., and Guruswamy, G. P., "Convergence Acceleration of an Aeroelastic Navier–Stokes Solver," AIAA Paper 94-2268, June 1994.